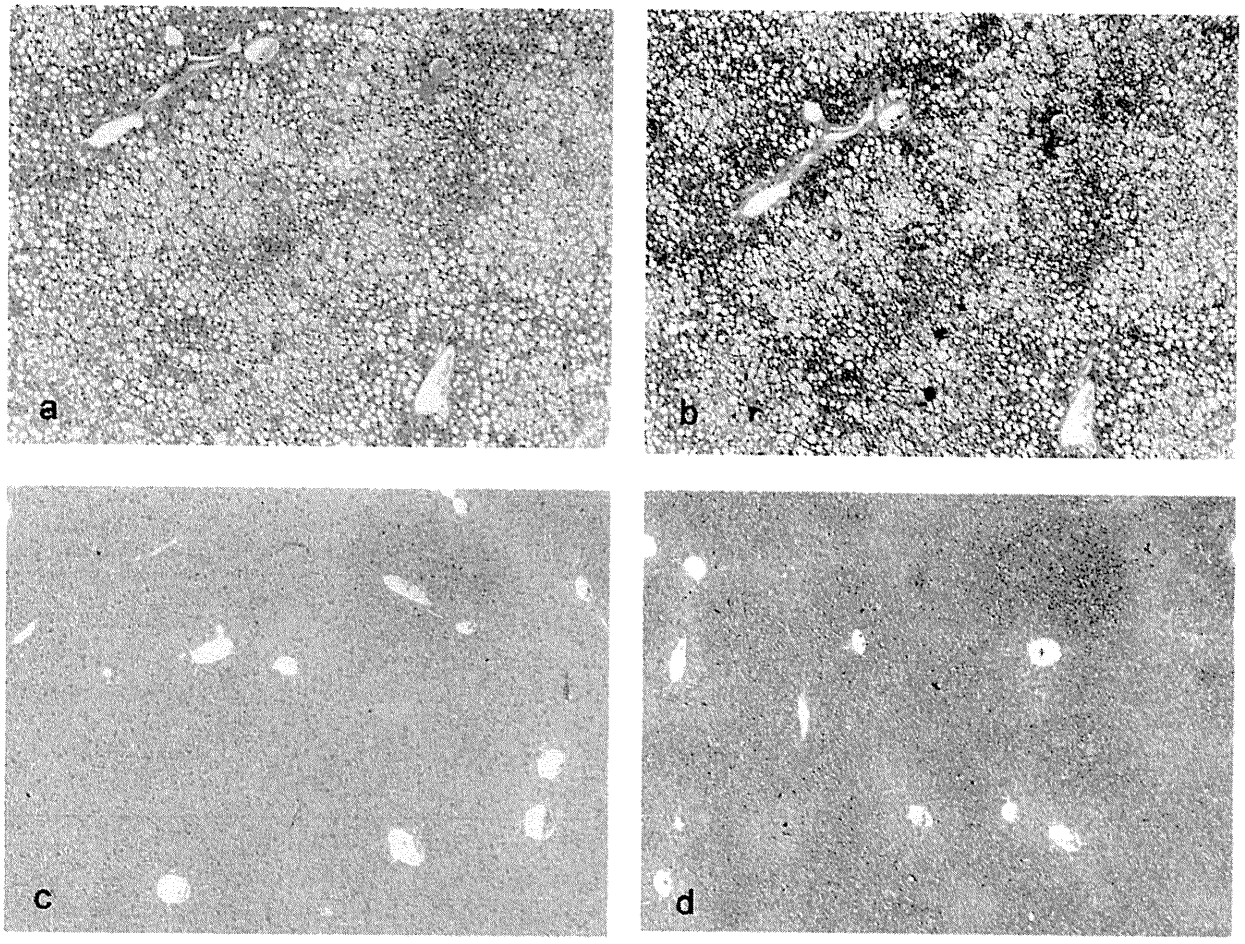

Figure 2. Histological futures of liver specimens. (a) Mouse treated with 0.005% ascorbic acid for 12 weeks. Hematoxylin-eosin stain, x100. (b) Mouse treated with 0.005% ascorbic acid for 12 weeks; Azan-Mallory stain, x100. (c) Mouse treated with 0.005% ascorbic acid and 0.1% EGCG for 12 weeks; Hematoxylin-eosin stain, x100. (d) Mouse treated with 0.005% ascorbic acid and 0.1% EGCG for 12 weeks; Azan-Mallory stain, x100. Immunoreactive products for anti-8-OhdG antibody localized in the cytoplasm of hepatocytes, especially deformed hepatocytes with fat droplets. Liver tissues of mice treated with 0.005% ascorbic acid for 12 weeks show histological features of typical NASH. However, those of mice with 0.005% ascorbic acid and 0.1% EGCG are similar to normal liver.

Immunohistochemistry. Immunoreactive products of 8-hydro-2'-deoxyguanosine (8-OhdG), a marker of oxidative DNA damage, in the liver were examined. Paraffin sections were incubated overnight with mouse monoclonal anti-8-OhgG antibody (Japan Institute for the Control of Aging, Fukuroi, Japan), followed by incubation with alkaline phosphatase-labeled horse antimouse IgG (Vector, Burlingame, CA) and visualization by diamnobenzidine. The degree of 8-OhdG immunolocalization in the liver tissues was categorized as 0, 1, 2 or 3. That is, 0, none in liver tissue; 1, <1/3 in the intrahepatic lobules; 2, 1/3-2/3 in the intrahepatic lobules; and 3, >2/3 in the intrahepatic lobules.

Western blotting. Western blotting was performed using anti-insulin receptor (IR), anti-insulin receptor substrate (IRS)-1 and anti-phosphorylated IRS-1 (pIRS-1), anti-pGSK3α/ß antibodies for insulin signaling, and using anti-Akt, -pAkt, -IκBα, -pIκBα, -NF-κB and -pNF-κB antibodies for TNF-α signaling in liver tissues. Whole extracts were prepared from liver tissues using Triton lysis buffer-containing protease and phosphatase inhibitors. Protein concentration of the extracts was determined, and 40 μg of protein was electrophorased on 10% SDS-polyacrylamide gels. The gels were then blotted onto the nitrocellulose membrane.

Statistical analysis. Numerical data were expressed as means ±SD. Student's t test was performed to assess statistical significance among each group. P-values <0.05 were considered significant.

Results

Changes of body weight of mice in the four groups. Body weight of mice in the four groups gradually increased throughout the course of the experiment period as shown in Fig. 1, but there was no significant difference among each group.

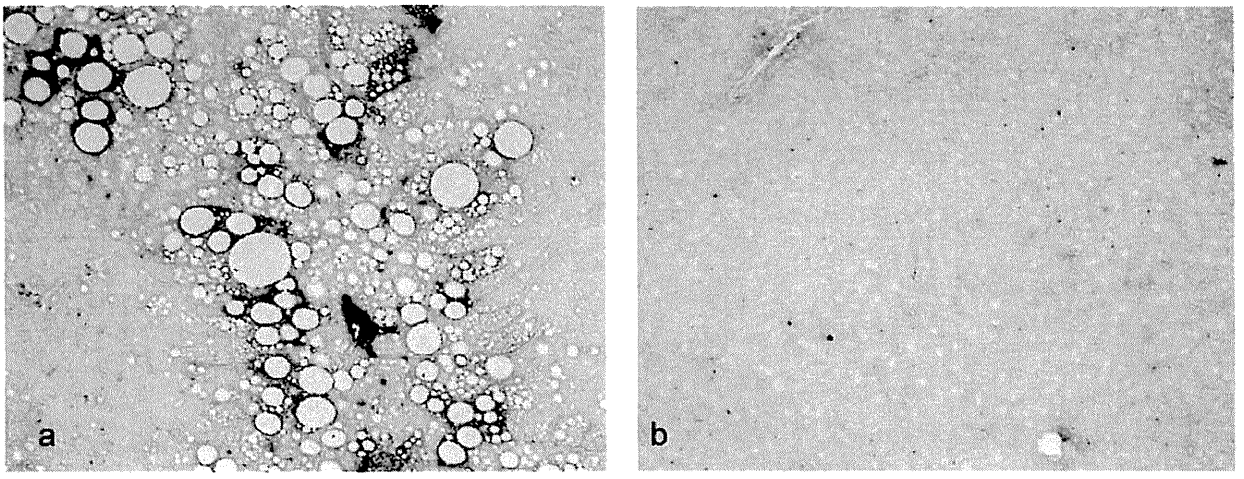

Figure 3. 8-OhdG immunolocalization in liver tissues. (a) 8-OhdG immunolocalization in the liver tissues of the 0.005% ascorbic acid-treated group is at grade 3, x100. (b) 8-OhdG immunolocalization in the liver tissues of the 0.005% ascorbic acid and 0.1% EGCG-treated group is at grade 1, x100. The degree of 8-OhdG immunolocalization in the liver tissues of the 0.005% ascorbic acid and 0.1% EGCG-treated group is low compared with that of other groups.

Ratio of liver weight to body weight at week 43. Ratio (percentage of expression) of liver weight to body weight in the high dose EGCG-treated group (group 4) was lowest compared with that of other groups (group 1, 12.8±2; group 2, 15.2±1.8; group 3, 12.4±5.6; and group 4, 7.2±4.8), and the difference between group 4 and groups 1 and 2 was significant ($p<0.05$ and <0.01, respectively) (Table I).

Biochemical assays containing serum biological markers. Blood ALT, total cholesterol, triglyceride and phospholipid levels of group 4 were significantly low compared with those of groups 1 and 2 ($p<0.05$, respectively) (Table I). The elevation of serum ALT, AST levels by EGCG treatment was not recognized. In addition, there were no significant differences between AST, free fatty acid, and glucose levels between any of the groups.

Morphometry of liver specimens. The degrees of steatosis, intralobular fibrosis, ballooning hepatocyte appearance and Mallory-Denk body appearance in group 4 significantly decreased compared with those in other groups ($p<0.05$) (Table II, Fig. 2).

Immunohistochemistry. Immunoreactive products for anti-8-OhdG antibody localized in the cytoplasm of hepatocytes, especially deformed hepatocytes with fat droplets (Fig. 3). The 8-OhdG immunolocalization in liver tissues of group 4 showed an obvious decrease compared with those of other groups, and the difference between the degree of 8-OhdG immunolocalization in group 4 and that of groups 2 and 3 was significant ($p<0.05$) (Table II, Fig. 3).

Western blotting. In Western blotting, the expressions of IR and pIRS-1 in liver tissues of group 4 increased compared with those of other groups. On the other hand, the expressions of pAkt, pIKKß and pNF-κB in liver tissues of group 4 decreased compared with those of other groups (Fig. 4).

Table II. Morphometry of liver tissues and degree of 8-OhdG immunolocalization in each group.

Group	1	2	3	4
Steatosis	2.9±0.4[a]	3.0±0[a]	2.4±0.5[a]	1.0±1.0
Ballooning hepatocyte	1.3±0.5[a]	2.0±0[a]	1.0±0[a]	0.4±0.5
Mallory-Denk body	0.9±0.4[a]	1.8±0.4[a]	0.8±0.4[a]	0.4±0.5
Fibrosis	1.3±0.8	1.0±0.7	1.2±0.4	0.8±1.1
8-OhdG localization	1.4±0.5	2.2±1.1[a]	1.8±1.3[a]	1.2±0.4

Group 1, mice given distilled water alone (n=6); group 2, mice given distilled water containing 0.005% ascorbic acid alone (n=6); group 3, mice given distilled water containing 0.005% ascorbic acid and low dose EGCG (0.05%) (n=6); group 4, mice given distilled water containing 0.005% ascorbic acid and high dose EGCG (0.1%) (n=6). EGCG, epigallocatechin-3-gallate: [a]$p<0.05$ compared with group 4.

Discussion

Nonalcoholic fatty liver disease (NAFLD) is associated with metabolic syndrome. The metabolic syndrome is characterized by insulin resistance, which is produced by a complex interaction between genetic factors, macronutrient intake and lifestyle that alters the cytokine profile, cell biology and biochemical milieu of the liver, adipose tissue and striated muscle. The resultant disequilibrium in lipid homeostasis causes triglycerides to accumulate in the liver (16). An increase in oxidative stress, due to the generation of reactive oxygen species as a result of mitochondrial abnormalities and induction of the cytochrome P-450 system is one mechanism by which the nonalcoholic fatty liver develops into NASH (4). The pathogenesis of cytologic ballooning and Mallory-Denk body formation and their role in NAFLD remain to be defined. In addition, inflammation and fibrosis are likely to be secondary to cirrhosis, hepatocellular carcinoma and death (2,3,17).

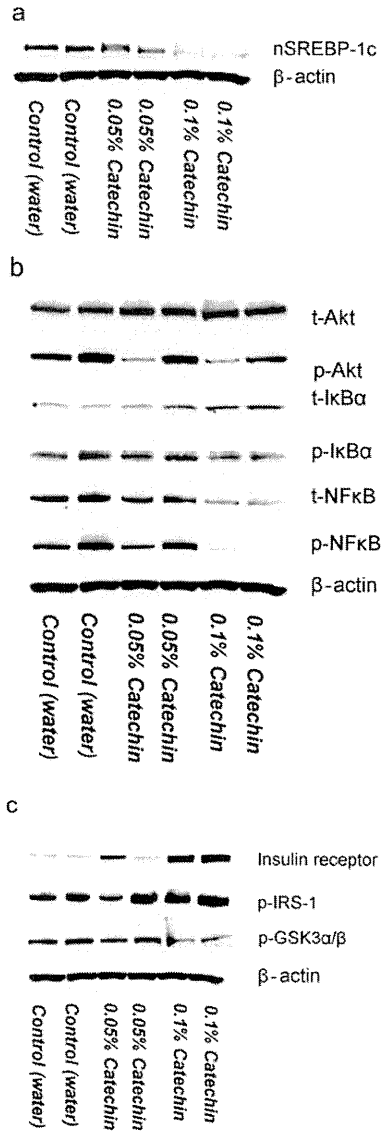

Figure 4. Western blotting. IκB, Inhibitor of κB; NF-κB: nuclear factor κB; t, total; p, phospholylated; IRS, insulin receptor substrate; GSK, glycogen synthase kinase. For Western blotting, the expressions of IR and pIRS-1 in liver tissues of group 4 increased compared with those of other groups. On the other hand, the expressions of pAkt, pIKKß and pNF-κB in group 4 decrease compared with those of other groups.

EGCG is an antioxidant and chemopreventional polyphenol that is found in green tea. It blocks activation of Ap-1 or NF-κB (18). EGCG has shown the inhibition of activation of IKKα, phosphorylation and subsequent degradation of IκBα (18). In addition, EGCG suppresses the proliferation of hepatic stellate cells and production of extracellular matrix in the hepatic fibrosis (19-21). Yumei *et al* reported that EGCG induced the *de novo* synthesis of glutathione and antifibrogenic effects in passaged rat hepatic stellate cells (22,23).

In the present study, green tea polyphenols containing EGCG showed effects of reducing inflammation, insulin resistance and oxidative stress (24-26), and improved the liver injury of transgenic mice expressing nSREBP-1c in the adipose tissue. EGCG inhibits nSREBP-1c expression in adipose tissues and Akt, IκBα and NF-κB expressions of liver tissues, and improves the insulin resistance of the liver tissues by promoting the functional recovery of the insulin receptor, insulin receptor substrate-1 (IRS-1) and glycogen synthase kinase (GSK) in the nSREBP-1c transgenic NASH model mice. The direct effect of EGCG to this model mouse is unclear. Its mechanism is likely due to the antioxidant and chemoprevention effects of EGCG (18).

Ingestion of tea rich catechins leads to a reduction in body fat and malondialdehyde-modified LDL in men (27). In obese individuals, body fat mainly accumulates in submucosal and visceral adipose tissue. Obesity alters both the cellular composition and function of adipose tissue. Adipose tissue of obese individuals contains an increased number of macrophages. Macrophages, adipocytes, and other cellular components of adipose tissue produce numerous circulating inflammatory markers including pro- and anti-inflammatory factors, chemokines, growth factors, and proteases that include a systemic inflammatory state and insulin resistance seen in individuals with increased body mass index (28). In this study, there is no significant difference among the four groups for body weight. Probably, the visceral adipose tissue of nSREBP-1c transgenic mice is less than that of wild type C57BL6 mice, and the significant difference is not recognized among each group.

The liver component of this metabolic disorder is NAFLD, which includes a spectrum of liver pathology ranging from steatosis to cirrhosis. Steatosis is often seen in obese individuals, and both presence and severity of steatosis correlate positively with adiposity. Increased hepatic free fatty acid oxidation that occurs in steatotic livers increases the generation of reactive oxygen species. Increased hepatocyte exposure to reactive oxygen species generates a state of oxidant stress and mitochondrial dysfunction, including hepatocellular injury and activation of hepatic stellate cells (HSC). In NAFLD, intestine-originated endotoxin accumulates the substance in the liver rather than to escape from liver. Increased levels of glucose and insulin up-regulate the synthesis of transforming growth factor-ß, angiotensin II, leptin, adiponectin and so on by HSC (29-31), and develop to the hepatic fibrosis.

In this study, there was no evidence of side effects by EGCG treatment. It will be important to clearly determine whether EGCG or green tea consumption can be used as a tool to prevent the development of NASH.

Acknowledgements

This research was supported by a Grant-in-Aid from the University and Society Collaboration and from COE Research from the Ministry of Education, Culture, Sports, Science and Technology of Japan.

References

1. Yoshiike N and Lwin H: Epidemiological aspects of obesity and NASH/NAFLD in Japan. Hepatol Res 33: 77-82, 2005.
2. Hashimoto E, Yatsuji S, Kaneda H, Yoshioka Y, Taniai M, Tokushige K and Shiratori K: The characteristics and natural history of Japanese patients with nonalcoholic fatty liver diseases. Hepatol Res 33: 72-76, 2005.

3. Ono M and Saibara T: Clinical features of nonalcoholic steatohepatitis in Japan: evidence from the literature. J Gastroenterol 41: 725-732, 2006.
4. Harrison SA, Kadakia S, Lang KA and Schenker S: Nonalcoholic steatohepatits: what we know in the new millennium. Am J Gastroenterol 97: 2714-2724, 2002.
5. Ludwig J, Viggiano TR, McGill DB and Ott BJ: Nonalcoholic steatohepatitis Mayo Clinic experiences with a hitherto unnamed disease. Mayo Clin Proc 55: 434-438, 1980.
6. Powel EE, Cooksley WG, Hanson R, Searle J, Halliday JW and Powell JW: The natural history of steatohepatitis: a follow-up study of forty-two patients for up to 21 years. Hepatology 11: 74-80, 1990.
7. Yoshioka Y, Hashimoto E, Yatsuji S, Kaneda H, Taniai M, Tokushige K and Shiratori K: Nonalcoholic steatohepatitis: cirrhosis, hepatocellular carcinoma and burnt-out NASH. J Gastroenterol 39: 1215-1218, 2004.
8. Bugianesi E, Leone N, Vanni E, Marchesini G, Brunello F, Carucci P, Musso A, De Paolis P, Capussotti L, Salizzoni M and Rizzetto M: Expanding the natural history of NASH: from cryptogenic cirrhosis to hepatocellular carcinoma. Gastroenterology 123: 134-140, 2002.
9. Nakayama H, Otabe S, Ueno T, Hirota N, Yuan X, Fukutani T, Hashinaga T, Wada N and Yamada K: Transgenic mice expressing nuclear sterol regulatory element-binding protein 1c in adipose tissue exhibit liver histology similar to nonalcoholic steatohepatitis. Metabolism 56: 470-475, 2007.
10. Bose M, Lambert JD, Ju J, Reuhl KR and Shapses SA: The major green tea polyphenol, (-)-epigallocatechin-3-gallate, inhibits obesity, metabolic syndrome, and fatty liver disease in high-fat-fed mice. J Nutr 138: 1677-1683, 2008.
11. Lee SM, Kim CW, Kim JK, Shin HJ and Baik JH: GCG-rich tea catechins are effective in lowering cholesterol and triglyceride concentrations in hyperlipidemic rats. Lipids 43: 419-429, 2008.
12. Murase T, Nagasawa A, Suzuki J, Hase T and Tokimitsu I: Beneficial effects of tea catechins on diet-induced obesity: stimulation of lipid catabolism in the liver. Int J Obes 26: 1459-1464, 2002.
13. Shimomura I, Hammer RE, Richardson JA, Ikemoto S, Bashmakov Y, Goldstein JL and Brown MS: Insulin resistance and diabetes mellitus in transgenic mice expressing nuclear SREBP-1c in adipose tissue: model for congenital generalized lipodystrophy. Genes Dev 12: 3182-3194, 1998.
14. Matteoni CA, Younossi ZM, Gramlich T, Boparai N, Liu YC and McCullough AJ: Nonalcoholic fatty liver disease: a spectrum of clinical and pathological severity. Gastroenterology 116: 1413-1419, 1999.
15. Kleiner DE, Brunt EM, Van Natta M, Behling C, Contos MJ, Cummings OW, Ferrell LD, Liu YC, Torbenson MS, Unalp-Arida A, Yeh M, McCullough AJ and Sanyal AJ: Nonalcoholic Steatohepatitis Clinical Research Network. Design and validation of a histological scoring system for nonalcoholic fatty liver disease. Hepatology 41: 1313-1321, 2005.
16. Korenblat KM, Fabbrini E, Mohammed BS and Klein A: Liver, muscle, and adipose tissue insulin action is directly related to intrahepatic triglyceride content in obese subjects. Gastroenterology 134: 1369-1375, 2008.
17. Sanyal AJ: Mechanisms of disease: pathogenesis of nonalcoholic fatty liver disease. Nat Clin Pra Gastroenterol Hepatol 2: 46-53, 2005.
18. Surh YJ: Cancer chemoprevention with dietary phytochemicals. Nat Rev Cancer 3: 768-780, 2003.
19. Sakata R, Ueno T, Nakamura T, Sakamoto M, Torimura T and Sata M: Green tea polyphenol epigallocatechin-3-gallate inhibits platelet-derived growth factor-induced proliferation of human hepatic stellate cell line LI90. J Hepatol 40: 52-59, 2004.
20. Chen A, Zhang L, Xu J and Tang J: The antioxidant (-)-epigallocatechin-3-gallate inhibits activated hepatic stellate cell growth and suppresses acetaldehyde-induced gene expression. Biochem J 368: 695-704, 2002.
21. Zhen M, Wang Q, Huang X, Cao L, Chen X, Sun K, Liu YJ, Li W and Zhang LJ: Green tea polyphenol epigallocatechin-3-gallate inhibits oxidative damage and preventive effects on carbon tetrachloride-induced hepatic fibrosis. J Nutr Biochem 18: 795-805, 2007.
22. Yumei F, Zhou Y, Zheng S and Chen A: The antifibrogenic effect of (-)-epigallocatechin gallate results from the induction of de novo synthesis of glutathione in passaged rat hepatic stellate cells. Lab Invest 86: 697-709, 2006.
23. Fu Y, Zheng S, Lu SC and Chen A: Epigallocatechin-3-gallate inhibits growth of activated hepatic stellate cells by enhancing the capacity of glutathione synthesis. Mol Pharmacol 73: 1465-1473, 2008.
24. Csala M, Margitti E, Senesi S, Gamberucci A, Banhegyi G, Mandl J, *et al*: Inhibition of hepatic glucose 6-phosphatase system by the green tea flavanol epigallocatechin gallate. FEBS Lett 581: 1693-1698, 2007.
25. Collins QF, Liu H, Pi J, Liu Z, Quon MJ and Cao W: Epigallocatechin-3-gallate (EGCG), a green tea polyphenol, suppresses hepatic gluconeogenesis through 5'-AMP-activated protein kinase. J Biol Chem 282: 30143-30149, 2007.
26. Igarashi K, Honma K, Yoshinari O, Nanjo F and Hara Y: Effects of dietary catechins on glucose tolerance, blood pressure and oxidative status in Goto-Kakizaki rats. J Nutr Sci Vitaminol 53: 496-500, 2007.
27. Nagao T, Komine Y, Soga S, Meguro S, Hase T, Tanaka Y and Tokimitsu I: Ingestion of a tea rich in catechins leads to a reduction in body fat and malondialdehyde-modified LDL in men. Am J Clin Nutr 81: 122-129, 2005.
28. Angulo P: NAFLD, obesity, and bariatric surgery. Gastroenterology 130: 1848-1852, 2006 .
29. Bataller R, Sancho-Bru P, Gines P and Brenner DA: Liver fibrogenesis: a new role for the rennin-angiotensin system. Antioxid Redox Signal 7: 1346-1355, 2005.
30. Ding X, Saxena NK, Lin S, Xu A, Srinivasan S and Ananina FA: The roles of leptin and adiponectin: a novel paradigm in adipocytokine regulation of liver fibrosis and stellate cell biology. Am J Pathol 166: 1655-1669, 2005.
31. Oben JA, Roskams T, Yang S, Lin H, Sinelli N, Torbenson M, Smedh U, Moran TH, Li Z, Huang J, Thomas SA and Diehl AM: Hepatic fibrogenesis requires sympathetic neurotransmitters. Gut 53: 438-445, 2004.

Hepatol Int (2011) 5:850–856
DOI 10.1007/s12072-010-9249-4

ORIGINAL ARTICLE

Safety and tolerance of sorafenib in Japanese patients with advanced hepatocellular carcinoma

Sadahisa Ogasawara · Fumihiko Kanai · Shuntaro Obi · Shinpei Sato · Taketo Yamaguchi · Ryosaku Azemoto · Hideaki Mizumoto · Youhei Koushima · Naoki Morimoto · Nobuto Hirata · Takeshi Toriyabe · Yusuke Shinozaki · Yoshihiko Ooka · Rintaro Mikata · Tetsuhiro Chiba · Shinichiro Okabe · Fumio Imazeki · Masaharu Yoshikawa · Osamu Yokosuka

Received: 9 August 2010 / Accepted: 30 December 2010 / Published online: 22 January 2011

Abstract

Purpose Sorafenib provides a survival benefit for patients with advanced hepatocellular carcinoma (HCC). However, there has been little experience with it in Japan. This study evaluated the safety and tolerance of sorafenib in Japanese patients with HCC.

Methods Clinical data for patients given sorafenib for advanced HCC were captured from eight institutions. All patients were classified as Child-Pugh A and the treatment was started at 400 mg twice daily. We recorded adverse events, treatment duration, and survival retrospectively. Adverse events were graded using Common Terminology Criteria, version 3.0; tumor response was assessed according to Response Evaluation Criteria in Solid Tumor, version 1.1.

Results Of the 54 patients treated, their median age was 69 years (range 48–82), 91% were males, 52% had HCV infection, and 22% had HBV infection. The most common drug-related adverse events were hand–foot skin reactions (HFSR) (72%), aspartate transaminase elevation (55%), alanine aminotransferase elevation (52%), rash (50%), fatigue (41%), and diarrhea (32%). Liver failure occurred in 19%. The median time to treatment failure was 2 months. Dose reduction was required in 83% of the patients, and this occurred within 2 weeks in 44%. The median overall survival was 6.9 months.

Conclusions These data suggest that sorafenib is generally tolerated in Japanese patients with HCC. Nevertheless, the majority needed a dose reduction. Adverse events including HFSR, rash, and liver failure occurred more frequently in our patients than those reported elsewhere. Careful attention must be paid to these adverse events during sorafenib administration.

S. Ogasawara · F. Kanai (✉) · T. Toriyabe · Y. Shinozaki · Y. Ooka · R. Mikata · T. Chiba · S. Okabe · F. Imazeki · M. Yoshikawa · O. Yokosuka
Department of Medicine and Clinical Oncology, Graduate School of Medicine, University of Chiba, 1-8-1 Inohana, Chuo-ku, 260-8670 Chiba, Japan
e-mail: kanaif@faculty.chiba-u.jp

S. Obi · S. Sato
Department of Gastroenterology and Hepatology, Kyoundo Hospital, 1-8 Kandasurugadai, Chiyoda-ku, 101-0062 Tokyo, Japan

T. Yamaguchi
Department of Gastroenterology, Chiba Cancer Centre, 666-2 Nitonacho, Chuo-ku, 260-8717 Chiba, Japan

R. Azemoto
Department of Gastroenterology, Kimitsu-Chuo Hospital, 1010 Sakurai, 292-8535 Kisarazu, Japan

H. Mizumoto
Department of Gastroenterology, Funabashi Municipal Medical Centre, 1-21-1 Kanasugi, 273-8588 Funabashi, Japan

Y. Koushima
Department of Gastroenterology, Saitama Red Cross Hospital, 8-3-33 Kamiochiai, Chuo-Ku, 333-8533 Saitama, Japan

N. Morimoto
Department of Gastroenterology, Shimotsuga-Sogo Hospital, 5-32 Fujimi, 328-8505 Tochigi, Japan

N. Hirata
Department of Gastroenterology, Kameda Medical Centre, 929 Higashicho, 296-0042 Kamogawa, Japan

Keywords Hepatocellular carcinoma · Sorafenib · Safety · Tolerance · Japanese

Introduction

Hepatocellular carcinoma (HCC) is the fifth most common cancer worldwide [1]. HCC develops mostly in patients with liver cirrhosis, which is typically caused by hepatitis C virus (HCV) infection, hepatitis B virus (HBV) infection, or alcohol [2]. The annual incidence of HCC in HCV-positive liver cirrhosis and chronic hepatitis is 6–7% and 1–2%, respectively [2]. The risk of cancer developing from chronic hepatitis or cirrhosis depends on the degree of fibrosis [3]. The hepatocarcinogenesis in the patients with hepatitis viruses differs between HCV and HBV. HCC occurs frequently in the cirrhotic livers of patients with HCV-positive liver disease. By contrast, HCC often develops in chronic HBV infection in the absence of cirrhosis. HCC developing from HBV infection has a lower cirrhosis complication rate than does HCC developing from HCV infection.

The etiology of HCC varies regionally [4]. In the Asia-Pacific region, except Japan, 70% of HCC is HBV-related and 20% is HCV-related [5]. In contrast, in Japan, 71–75% of HCC is HCV-related [2, 6]. The incidence of HCV infection is also increasing in the USA and Europe, as is the incidence of HCC [7].

Both surgical resection and local ablation therapy, including radiofrequency ablation, are considered curative for HCC [8–10]. Transarterial chemoembolization (TACE) has been applied to patients with advanced incurable HCC [11, 12]. However, the majority of patients experience recurrence or metastasis after these treatments. Although systemic therapy is available for advanced HCC, the prognosis remains poor. No standard systemic therapy that prolongs survival had been indentified before sorafenib was approved.

Sorafenib, an oral multikinase inhibitor, blocks tumor cell proliferation by targeting Raf/MEK/ERK signaling at the level of Raf kinase, and exerts an antiangiogenic effect by targeting vascular endothelial growth factor receptor-beta (VEGFR-β, PDGF-β) tyrosine kinases [13]. The Sorafenib HCC Assessment Randomized Protocol (SHARP) and Asia-Pacific studies demonstrated a significant survival benefit and good tolerance in patients with advanced HCC, making sorafenib the new reference standard for systemic therapy of patients with advanced HCC [14, 15]. In the SHARP study, approximately 90% of the patients were enrolled from Europe [14], and the Asia-Pacific study was conducted in China, Taiwan, and South Korea [15], but not Japan. The sorafenib groups in the SHARP and Asia-Pacific studies reflected the geographic patient pools, including HCV infection (29 vs. 10.7%) and HBV infection (19 vs. 70.7%) [14, 15]. In both studies, baseline disease characters differed from those of Japanese HCC patients. HCV-related HCC is most common in Japan, as mentioned above, and most of these patients have hepatitis or cirrhosis due to HCV.

In Japan, a phase I study evaluated the pharmacokinetics, safety, and preliminary efficacy of sorafenib in HCC patients [16]. Then, based on the results of the SHARP and Asia-Pacific studies, together with the phase I study in Japanese HCC, the use of sorafenib to treat HCC patients was approved by the Japanese Ministry of Health, Labour, and Welfare in May 2009 [14–16]. However, the phase I study included few patients (six Child-Pugh A patients and eight Child-Pugh B patients receiving 400 mg twice daily) [16]. Thus, little is, in fact, known about the safety and tolerance profile of sorafenib in Japanese HCC patients. In this study, we evaluated the safety and tolerance of sorafenib in Japanese HCC patients.

Materials and methods

HCC patients treated with sorafenib between May 2009 and December 2009 at eight medical centers in Japan were analyzed retrospectively. Patients were required to meet the following criteria at baseline: (1) diagnosis of HCC based on the European Association for the Study of Liver Disease/American Association for Liver Disease criteria or liver histology [8]; (2) Eastern Cooperative Oncology Group Performance Status (ECOG-PS) 0, 1, or 2; (3) classified as Child-Pugh A; (4) required to have adequate renal, hematological, and hepatic function (platelet count $\geq 50 \times 10^9$/L, hemoglobin concentration $\geq$8.5 g/L, albumin concentration $\geq$2.8 g/L, total bilirubin concentration $\leq$3.0 mg/dL, alanine aminotransferase (ALT) concentration $\leq$5 times the upper limit of normal (ULN), serum creatinine concentration $\leq$1.5 times the ULN, and prothrombin time-international normalized rate (INR) $\leq$2.3. Patients who received 400 mg sorafenib twice daily as an initial dose were selected, and treatment interruptions and dose reductions (first to 400 mg once daily, and then to 400 mg once every other day) were allowed for the toxicity study. Dose reduction and treatment discontinuation were based on the package insert and were required for drug-related toxicities. For grade 3/4 toxicities, patients received a lower dose when the toxicity improved to grade 2 or better, but therapy was discontinued if the recovery time was 30 days or longer. Dose reduction was introduced for grade 3 non-hematologic toxicities until the toxicity was grade 2 or better; patients were then treated at one dose

level lower, and therapy was discontinued if the recovery time was 30 days or longer. Treatment was discontinued for patients with drug-related grade 4 non-hematologic toxicities. However, a modified scale resulting from a phase II trial was used for skin toxicity [17].

We recorded demographics, prior therapy, plasma α-fetoprotein (AFP) level, existence of microvascular invasion, or extrahepatic spread of HCC, Barcelona Clinic Liver Cancer (BCLC) score, tumor response, survival data, and relevant toxicities.

Adverse events were recorded according to the Common Terminology Criteria for Adverse Events, version 3.0 (CTCAE v3.0). Based on contrast-enhanced computed tomography (CT) or contrast-enhanced magnetic resonance imaging (MRI), performed at baseline and 1–3 months after treatment, the tumor response was evaluated using the Response Evaluation Criteria in Solid Tumors criteria version 1.1 (RECIST v1.1). The duration of treatment and survival were estimated using the Kaplan–Meier method.

Results

Patient baseline characteristics

In total, 54 patients were included in this retrospective study. Their median age was 69 years (range 48–82), and 49 patients (91%) were males. Most had good performance status (ECOG-PS was 0 in 81% and 1 in 15% of patients). At baseline, 28 patients (52%) had HCV infection and 12 patients (22%) had HBV infection. Of the patients, 38 (70%) were classified as BCLC stage C and 28 patients (52%) had extrahepatic metastases. Before receiving sorafenib therapy, 50 patients (93%) had been treated with surgery, local ablation, or TACE (Table 1).

Table 1 Baseline demographics and disease characteristics of the enrolled patients

Number of patients	54
Sex, no. (%)	
Male	49 (91)
Female	5 (9)
Age (years)	
Median (range)	69 (48–82)
Body weight (kg)	
Median (range)	60.8 (43.6–81.3)
Body surface area ($m^{2)}$	
Median (range)	1.66 (1.32–1.93)
ECOG PS, no. (%)	
0	44 (81)
1	8 (15)
2	2 (4)
Child-Pugh score, no. (%)	
5	36 (67)
6	18 (33)
Hepatitis virus status, no. (%)	
HCV infection	28 (52)
HBV infection	12 (22)
Alcohol	8 (15)
Other	6 (11)
BCLC stage, no. (%)	
B (intermediate)	16 (30)
C (advanced)	38 (70)
Macroscopic vascular invasion, no. (%)	12 (22)
Extrahepatic spread, no. (%)	
Any	28 (52)
Lymph nodes	8 (15)
Lung	14 (26)
Bone	6 (11)
Prior treatment, no. (%)	
Any	50 (93)
Surgery	27 (50)
Local ablation	25 (46)
Transarterial chemoembolization	43 (80)
Biochemical analysis, median (range)	
Platelets/mm^3	133,500 (50,000–296,000)
Albumin (g/dL)	3.7 (2.8–4.9)
Total bilirubin (mg/dL)	0.8 (0.2–1.9)
Aspartate aminotransferase (AST) (IU/L)	51 (18–176)
Alanine aminotransferase (ALT) (IU/L)	40 (11–162)
Alpha fetoprotein (AFP) (ng/mL)	246.6 (2.8–184,100.0)

Safety and tolerability

The overall incidence of drug-related adverse events of any grade was 98% and 36 patients (68%) experienced grade 3/4 adverse events (Table 2). HFSR occurred in 39 patients (72%) and was grade 3/4 in 14 patients (26%). Rash occurred in 27 patients (50%) and was grade 3/4 in 7 patients (13%). Fatigue, diarrhea, and hypertension occurred in 22 (41%), 17 (32%), and 14 patients (26%), respectively; none of these toxicities was grade 3/4. Liver failure under treatment, defined as encephalopathy, massive ascites, or jaundice, occurred in ten patients (19%). The median average daily dose was 450 mg (range 182–800 mg). Dose reduction was required in 45 patients (83%) (Table 3). The most common adverse events leading to dose reduction were HFSR ($n = 21$, 38%), aspartate transaminase (AST)/ALT elevation ($n = 8$, 15%), rash ($n = 7$, 13%), and liver failure ($n = 4$, 7%). Treatment was discontinued in 17 patients (31%) for sorafenib intolerance (Table 4). The most frequent adverse events leading to

Table 2 Drug-related adverse events

	Any	Grade 3/4
Overall incidence	53 (98)	36 (68)
Hematological		
Hemoglobin	1 (2)	0
Leukocytes	4 (8)	0
Platelets	14 (26)	3 (6)
Dermatologic events		
Hand–foot skin reaction	39 (72)	14 (26)
Rash	27 (50)	7 (13)
Alopecia	9 (17)	
Gastrointestinal events		
Anorexia	12 (22)	4 (7)
Diarrhea	17 (32)	0
Vomiting	3 (6)	1 (2)
Fatigue	22 (41)	0
Voice changes	2 (4)	0
Hypertension	14 (26)	0
Abdominal pain not otherwise specified	5 (9)	0
Bleeding	4 (8)	2 (4)
Laboratory		
AST	30 (55)	13 (24)
ALT	28 (52)	8 (15)
Bilirubin	15 (28)	6 (11)
Amylase	15 (28)	3 (6)
Liver failure	10 (19)	

Liver failure is defined as encephalopathy, massive ascites, or jaundice

Table 3 Adverse events causing dose reduction

	Number of patients (%)
Patients requiring dose reduction	45 (83)
Hand–foot skin reaction	21 (38)
AST/ALT	8 (15)
Rash	7 (13)
Liver failure	4 (7)
Anorexia	2 (4)
Bleeding	2 (4)
Vomiting	1 (2)
Time to dose reduction	
<2 weeks	24 (44)
≥2 weeks to <4 weeks	12 (22)
≥4 weeks	9 (17)

treatment discontinuation were liver failure ($n = 4$, 7%), HFSR ($n = 4$, 6%), fatigue ($n = 3$, 6%), and abdominal pain not otherwise specified ($n = 3$, 6%). The median time to treatment failure (TTF; defined as the period from first treatment to discontinuation of sorafenib treatment, progression, or death) was 2 months (Fig. 1).

Table 4 Adverse events leading to treatment discontinuation

	Number of patients (%)
Any adverse events	17 (31)
Liver failure	4 (7)
Hand–foot skin reaction	3 (6)
Fatigue	3 (6)
Abdominal pain not otherwise specified	3 (6)
Anorexia	2 (4)
Rash	2 (4)

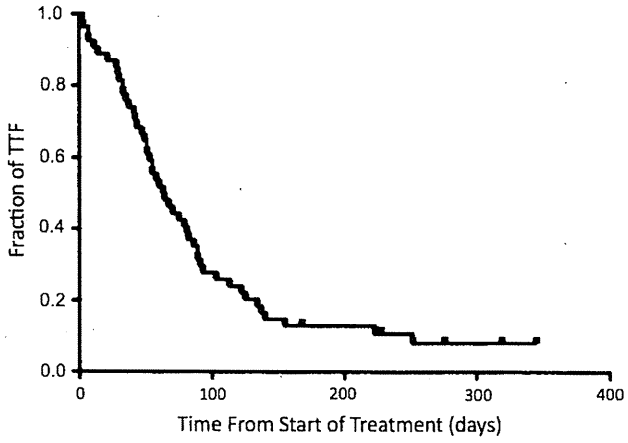

Fig. 1 Kaplan–Meier analysis of time to treatment failure (TTF). The median TTF was 2 months

Efficacy

According to RECIST version 1.1, one patient (2%) had a partial response, 25 patients had stable disease (57%), and the disease control rate (DCR; defined as no disease progression for ≥4 weeks) was 34% (Table 5).

At the time of analysis, with a median follow-up of 5.7 months (range 0.5–13.3), 49 patients had discontinued treatment (92%) and 28 patients were dead (52%). The overall median survival was 6.9 months (Fig. 2)

Discussion

The SHARP and Asia-Pacific studies, large, multicentre, phase III, randomized, double-blind, placebo-controlled trials of sorafenib, revealed a survival benefit and the tolerability of sorafenib in advanced HCC patients. However, considering the varying etiologies and treatment strategies for HCC in different regions [4], it is unclear whether these results apply to Japanese HCC patients. In Japan, high-risk groups for HCC, such as cirrhosis or hepatitis patients, undergo ultrasonography every 3–4 months and CT or MRI every 6–12 months for the early detection of HCC. Because we find HCC when it is earlier, Japanese HCC

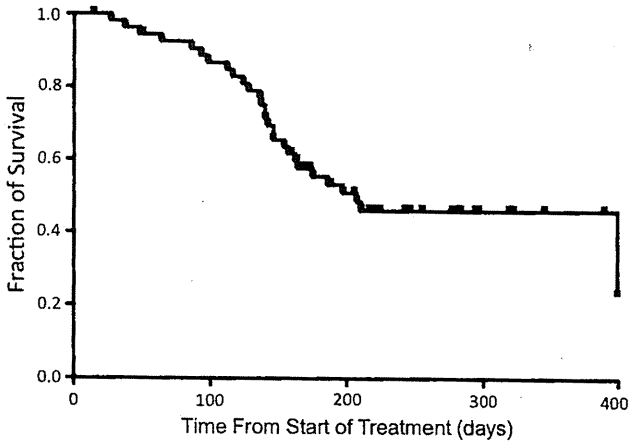

Fig. 2 Kaplan-Meier analysis of overall survival (OS). The median OS was 6.9 months

Table 5 Response rates using the response evaluation criteria in solid tumors

Response ($n = 44$)	Number of patients (%)
Complete response	0
Partial response	1 (2)
Stable disease	25 (57)
Progressive disease	18 (41)
DCR	15 (34)

DCR is the disease control rate, defined as the proportion of patients who had a best response rating of a complete response, partial response, or stable disease that was maintained for ≥4 weeks from the first manifestation of the rating

patients are often able to undergo surgery, local ablation, and TACE. Despite the efficacy of these procedures, patients frequently develop recurrence or disease progression after these treatments. In contrast, in much of the rest of Asia, the majority of patients are present with advanced disease, with large tumors, multiple tumors, and portal tumor thrombosis. These patients are less likely to receive curative treatment [18]. Furthermore, the liver function of HBV-related HCC patients tends to be better than that of HCV-related HCC patients. Shiratori et al. [2] reported that 38.6, 39.3, and 22.1% of cases presented as Child-Pugh A, B, and C when the severity of cirrhosis was classified in Japanese HCV-related HCC patients. By contrast, among the HBV-related HCC patients, 65.2, 26.1, and 8.7% cases presented as Child-Pugh A, B, and C. Additionally, liver function might worsen with the repetition of local therapies because sorafenib was only given to Child-Pugh A patients. Fewer HCV-related HCC patients (52%) were included in the present analysis compared with the general HCC prevalence in Japan (71–75%) [2, 6].

In the SHARP study, common drug-related adverse events were diarrhea (39%), fatigue (22%), HFSR (21%), rash (16%), alopecia (14%), anorexia (14%), and nausea (11%) [14]. Dose reduction due to adverse events was needed in 26% of subjects. The most common adverse events leading to dose reduction were diarrhea (8%), HFSR (5%), and rash (3%) [14]. Treatment was discontinued because of adverse events in 38%. The most frequent adverse events leading to sorafenib discontinuation were gastrointestinal events (6%), fatigue (5%), and liver dysfunction (5%) [14]. In comparison, in the Asia-Pacific study, the common drug-related adverse events were HFSR (45.0%), diarrhea (25.5%), alopecia (24.8%), fatigue (20.1%), rash (18.8%), hypertension (18.8%), and anorexia (12.8%) [15]. Dose reduction due to adverse events was needed in 30.9%, and treatment was discontinued due to adverse events in 19.5% [15]. The most common drug-related adverse events resulting in dose reduction were HFSR (11.4%) and diarrhea (7.4%) [15]. Compared with these studies, we observed a higher incidence of adverse events, especially HFSR, rash, hypertension, and liver failure.

The incidence of HFSR and rash in the Asia-Pacific study was higher than in the SHARP study [14, 15]. In a phase I study of a small population of Japanese patients with HCC, five of the six patients experienced HFSR and four experienced rash; these patients were Child-Pugh A receiving 400 mg twice daily [16]. In a phase II study of Japanese patients with advanced renal cell carcinoma [19], HFSR occurred in 55% and rash occurred in 37.4%. Asian patients, particularly Japanese, frequently develop HFSR. Although it is possible that the physiological difference is partly associated with race, prevention and management of HFSR are required in Japanese patients.

Regarding hypertension, Wu et al. [20] reported a 23.4% (95% CI 16.0–32.9%) overall incidence from a systemic review and meta-analysis of nine studies of renal cell cancer or other solid tumor. Hypertension was experienced by 14 patients (26%) in our study; no case was grade 3/4. Varying rates of hypertension have been reported, with a 5% incidence in the SHARP study and an 18.8% incidence in the Asia-Pacific study. In our study, the incidence of hypertension was comparable with that reported by Wu et al., although it was slightly higher compared with that reported in the SHARP and Asia-Pacific studies.

Liver failure occurred in ten patients (19%), while it was uncommon in the SHARP and Asia-Pacific studies. Nevertheless, Ozenne et al. [21] reported that seven (21%) French patients with Child-Pugh A experienced liver failure. The SHARP and Asia-Pacific studies showed the efficacy of sorafenib in carefully selected patients with advanced HCC. Liver failure may occur with the use of sorafenib in an unselected cirrhotic population. In our study, the median time to experience liver failure was 33 days (range 7–115); liver failure can happen in the

early days of treatment. Furthermore, a common adverse event leading to treatment discontinuation was liver failure (7%).

In our study, 43 patients required dose reduction due to adverse events (83%). This was more frequent than in either the SHARP or Asia-Pacific studies. The most common adverse event leading to dose reduction was HFSR (43%) [12, 13]. Our patients suffered more HFSR than those in the SHARP and Asia-Pacific studies [12, 13]. The cause may be differences, such as age or race. Nevertheless, treatment discontinuation due to HFSR was required in only 6% of the patients; in the majority of the patients, it could be controlled by dose reduction. This concurred with the finding that two of seven patients with Child-Pugh A experienced HFSR when they took 400 mg daily in the Japanese phase I study [16].

In our series, 44% of the patients required dose reduction within 2 weeks and the median daily dose was 450 mg (range 182–800), demonstrating that it is difficult for Japanese patients to continue sorafenib treatment at 400 mg twice daily. Treatment was discontinued because of adverse events in 31% of our patients, which was similar to the rate in the SHARP study, but higher than in the Asia-Pacific study. Adverse events could be managed by dose reduction in the majority of patients. Therefore, careful follow-up is recommended.

The median overall survival was 10.7 months in the SHARP trial and 6.5 months in the Asia-Pacific trial. The differences in survival time might have been caused by differences in patient background. Patients in the Asia-Pacific study displayed more extrahepatic spread, more hepatic tumors, a worse ECOG-PS, and increased concentrations of AFP compared with patients in the SHARP study [14, 15]. The median survival time was 9.2 months in a phase II study [17] and 15.6 months in a Japanese phase I study [16], although Child-Pugh B patients were included in both of these studies. More recently, two retrospective studies from Europe showed that the median survival times for Child-Pugh A patients were 8.9 [21] and 8.3 months [22]. The median overall survival in our series was 6.9 months, although the survival benefits cannot be directly compared, as this was a retrospective study. Our study included many patients with higher serum AFP levels, suggesting the inclusion of highly advanced cases in the present study.

In summary, the present study demonstrated that sorafenib was generally tolerated in Japanese HCC patients because the probability of treatment discontinuation due to adverse events was acceptable, although most patients needed dose reduction. The overall safety profile of sorafenib was similar to that seen in previous studies in patients with HCC, except for the higher rates of HFSR, rash, and liver failure.

Acknowledgements We want to thank Yu Yoshida, Kazuyoshi Nakamura, and Takao Nishikawa for their contributions.

References

1. Parkin DM, Bray F, Ferlay J, Pisani P. Global cancer statistics, 2002. CA Cancer J Clin 2005;55(2):74–108
2. Shiratori Y, Shiina S, Imamura M, Kato N, Kanai F, Okudaira T, Teratani T, Tohgo G, Toda N, Ohashi M, et al. Characteristic difference of hepatocellular carcinoma between hepatitis B- and C- viral infection in Japan. Part 1. Hepatology 1995;22(4): 1027–1033
3. Okuda H. Hepatocellular carcinoma development in cirrhosis. Best Pract Res Clin Gastroenterol 2007;21(1):161–173
4. Llovet JM, Burroughs A, Bruix J. Hepatocellular carcinoma. Lancet 2003;362(9399):1907–17
5. McGlynn KA, Tsao L, Hsing AW, Devesa SS, Fraumeni JF Jr. International trends and patterns of primary liver cancer. Int J Cancer 2001;94(2):290–296
6. Umemura T, Kiyosawa K. Epidemiology of hepatocellular carcinoma in Japan. Hepatol Res 2007;37(Suppl 2):S95–S100
7. El-Serag HB, Mason AC. Rising incidence of hepatocellular carcinoma in the United States. N Engl J Med 1999;340(10): 745–750
8. Ryu M, Shimamura Y, Kinoshita T, Konishi M, Kawano N, Iwasaki M, Furuse J, Yoshino M, Moriyama N, Sugita M. Therapeutic results of resection, transcatheter arterial embolization and percutaneous transhepatic ethanol injection in 3225 patients with hepatocellular carcinoma: A retrospective multicentre study. Jpn J Clin Oncol 1997;27(4):251–257
9. Okuda K, Mitchell DG, Itai Y. In Hepatobiliary Disease Primary Malignant Tumors of the Liver. London: Blackwell; 2001. 343–389
10. Bruix J, Sherman M, Llovet JM, Beaugrand M, Lencioni R, Burroughs AK, Christensen E, Pagliaro L, Colombo M, Rodes J. Clinical management of hepatocellular carcinoma. Conclusions of the Barcelona-2000 EASL conference. European Association for the Study of the Liver. J Hepatol 2001;35(3):421–430
11. Llovet JM, Real MI, Montana X, Planas R, Coll S, Aponte J, Ayuso C, Sala M, Muchart J, Sola R, Rodes J, Bruix J. Arterial embolisation or chemoembolisation versus symptomatic treatment in patients with unresectable hepatocellular carcinoma: a randomised controlled trial. Lancet 2002;359(9319):1734–1739
12. Takayasu K, Arii S, Ikai I, Omata M, Okita K, Ichida T, Matsuyama Y, Nakanuma Y, Kojiro M, Makuuchi M, Yamaoka Y. Prospective cohort study of transarterial chemoembolization for unresectable hepatocellular carcinoma in 8510 patients. Gastroenterology 2006;131(2):461–469
13. Wilhelm SM, Carter C, Tang L, Wilkie D, McNabola A, Rong H, Chen C, Zhang X, Vincent P, McHugh M, Cao Y, Shujath J, Gawlak S, Eveleigh D, Rowley B, Liu L, Adnane L, Lynch M, Auclair D, Taylor I, Gedrich R, Voznesensky A, Riedl B, Post LE, Bollag G, Trail PA. BAY 43–9006 exhibits broad spectrum oral antitumor activity and targets the RAF/MEK/ERK pathway and receptor tyrosine kinases involved in tumor progression and angiogenesis. Cancer Res 2004;64(19):7099–7109
14. Llovet JM, Ricci S, Mazzaferro V, Hilgard P, Gane E, Blanc JF, de Oliveira AC, Santoro A, Raoul JL, Forner A, Schwartz M, Porta C, Zeuzem S, Bolondi L, Greten TF, Galle PR, Seitz JF, Borbath I, Haussinger D, Giannaris T, Shan M, Moscovici M, Voliotis D, Bruix J. Sorafenib in advanced hepatocellular carcinoma. N Engl J Med 2008;359(4):378–390
15. Cheng AL, Kang YK, Chen Z, Tsao CJ, Qin S, Kim JS, Luo R, Feng J, Ye S, Yang TS, Xu J, Sun Y, Liang H, Liu J, Wang J, Tak

WY, Pan H, Burock K, Zou J, Voliotis D, Guan Z. Efficacy and safety of sorafenib in patients in the Asia-Pacific region with advanced hepatocellular carcinoma: a phase III randomised, double-blind, placebo-controlled trial. Lancet Oncol 2009;10(1):25–34
16. Furuse J, Ishii H, Nakachi K, Suzuki E, Shimizu S, Nakajima K. Phase I study of sorafenib in Japanese patients with hepatocellular carcinoma. Cancer Sci 2008;99(1):159–165
17. Abou-Alfa GK, Schwartz L, Ricci S, Amadori D, Santoro A, Figer A, De Greve J, Douillard JY, Lathia C, Schwartz B, Taylor I, Moscovici M, Saltz LB. Phase II study of sorafenib in patients with advanced hepatocellular carcinoma. J Clin Oncol 2006;24(26): 4293–4300
18. Yuen MF, Hou JL, Chutaputti A. Hepatocellular carcinoma in the Asia pacific region. J Gastroenterol Hepatol 2009;24(3):346–353
19. Akaza H, Tsukamoto T, Murai M, Nakajima K, Naito S. Phase II study to investigate the efficacy, safety, and pharmacokinetics of sorafenib in Japanese patients with advanced renal cell carcinoma. Jpn J Clin Oncol 2007;37(10):755–762
20. Wu S, Chen JJ, Kudelka A, Lu J, Zhu X. Incidence and risk of hypertension with sorafenib in patients with cancer: a systematic review and meta-analysis. Lancet Oncol 2008;9(2):117–123
21. Ozenne V, Paradis V, Pernot S, Castelnau C, Vullierme MP, Bouattour M, Valla D, Farges O, Degos F. Tolerance and outcome of patients with unresectable hepatocellular carcinoma treated with sorafenib. Eur J Gastroenterol Hepatol 2010;22(9): 1106–1110
22. Pinter M, Sieghart W, Graziadei I, Vogel W, Maieron A, Konigsberg R, Weissmann A, Kornek G, Plank C, Peck-Radosavljevic M. Sorafenib in unresectable hepatocellular carcinoma from mild to advanced stage liver cirrhosis. Oncologist 2009; 14(1):70–76

Cardiovasc Intervent Radiol (2011) 34:81–86
DOI 10.1007/s00270-010-9835-9

CLINICAL INVESTIGATION

Detection of Corona Enhancement of Hypervascular Hepatocellular Carcinoma by C-Arm Dual-Phase Cone-Beam CT During Hepatic Arteriography

Shiro Miyayama · Masashi Yamashiro · Miho Okuda · Yuichi Yoshie · Yoshiko Nakashima · Hiroshi Ikeno · Nobuaki Orito · Osamu Matsui

Received: 12 December 2009 / Accepted: 18 February 2010 / Published online: 24 March 2010

Abstract The purpose of this study was to evaluate the detectability of corona enhancement around the hypervascular hepatocellular carcinoma (HCC) by dual-phase cone-beam computed tomography during hepatic arteriography (CBCTHA). Dual-phase CBCTHA was performed for 71 HCC lesions (mean ± SD 1.7 ± 0.9 cm), including seven presenting a nodule-in-nodule appearance and nine hypervascular pseudolesions. The first scan was performed during injection of 30–40 ml half-diluted contrast material at a rate of 1.5–2 ml/s through the hepatic artery. Scanning was initiated 7 s after the beginning of contrast material injection. The second scan was started 30 s after the end of the first scan. Detectability of corona enhancement on second-phase CBCTHA was evaluated. Thickness of corona enhancement was also analyzed as thin (≤2 mm) or thick (>2 mm). Corona enhancement was detected in 63 (88.7%) of 71 tumors (1.8 ± 0.9 cm), but it was not detected in eight tumors (1.0 ± 0.2 cm). Thin corona enhancement was seen in 18 tumors (1.2 ± 0.5 cm), and thick corona enhancement was seen in 45 tumors (2.0 ± 0.9 cm). There was a significant difference in tumor diameter between tumors with and those without corona enhancement ($P = 0.0157$) and between thin and thick corona enhancement ($P = 0.001$). In all seven early-stage tumors, corona enhancement was demonstrated around the hypervascular focus within the hypovascular tumor portion. None of the nine pseudolesions showed any corona enhancement. Dual-phase CBCTHA depicted corona enhancement in 88.7% of hypervascular HCC lesions. This technique may improve the diagnostic accuracy of HCC.

Keywords Hepatocellular carcinoma · Corona enhancement · Cone-beam CT

S. Miyayama (✉) · M. Yamashiro · M. Okuda · Y. Yoshie · Y. Nakashima · H. Ikeno · N. Orito
Department of Diagnostic Radiology,
Fukuiken Saiseikai Hospital, Fukui 918-8503, Japan
e-mail: s-miyayama@fukui.saiseikai.or.jp

O. Matsui
Department of Radiology, Graduate School of Medical Science,
Kanazawa University, Kanazawa 920-8641, Japan

Introduction

Corona enhancement is one of the characteristic findings of hypervascular hepatocellular carcinoma (HCC) on late-phase computed tomography during hepatic arteriography (CTHA) and single-level dynamic CTHA [1–5]. On single-level dynamic CTHA, corona enhancement around the HCC lesion appears between 22 and 40 s after contrast material injection [1]. This finding is also helpful to distinguish between HCC and other hypervascular pseudolesions, such as arterioportal shunts, which do not require treatment [2].

C-arm cone-beam CT (CBCT) is an alternative technology for obtaining CT-like images using an angiographic unit equipped with a flat panel detector (FPD) [6–9]. We have applied this technique to assist transcathater arterial chemoembolization (TACE) for HCC. In our previous reports, CBCT during hepatic arteriography (CBCTHA) had sufficient image quality to detect almost all of the small HCC lesions [8, 9]. In our CBCT protocol (XperCT; Philips Medical Systems, Best, The Netherlands), the second CBCT scan could be performed 90 s after the end of the first scan, just as corona enhancement would be expected to disappear. Two separate scans and two contrast material injections may be necessary to depict both tumor

stain and corona enhancement; however, this may increase the procedural time and total amount of contrast material.

Recently, a prototype of dual-phase CBCT software has been made available by the manufacturer. In this report, the detectability of corona enhancement of HCC by dual-phase CBCTHA technique was analyzed.

Materials and Methods

Patients

Between August and October 2009, TACE for HCC was performed in 66 patients. Among these, we performed dual-phase CBCTHA in 30 patients with newly developed tumors <5 cm in diameter. Our Institutional Review Board approved the use of a prototype of the dual-phase CBCT software (Philips). Written informed consent was obtained from each patient before the procedure. There were 17 men and 13 women (mean patient age 72.1 ± 7.9 years [range 48–85]). All patients had chronic hepatitis or liver cirrhosis. This was related to hepatitis C in 21 patients and to hepatitis B in four patients. In one patient, cirrhosis was related to both hepatitis B and C. In another patient, it was related to alcoholism. The etiology was unknown in three patients. The diagnosis of HCC was established by CT and/or magnetic resonance imaging findings, i.e., characteristic nodular enhancement on the arterial-phase and wash out on delayed-phase images, in addition to nodular stain on angiography. All patients had 1–8 tumors (mean 2.4 ± 1.7). Seven tumors were early-stage HCC presenting hypervascular foci within a hypovascular tumor portion, a so called nodule-in-nodule appearance. In such tumors, the diameter of the hypervascular focus was defined as the tumor diameter. In total, 71 tumors with a mean diameter 1.7 ± 0.9 cm (range 0.8–4.6) were found. Nine hypervascular pseudolesions, such as arterioportal shunts that were defined as showing early enhancing lesions with an amorphous shape or wedge-shape on arterial-phase CT and isoattenuating on unenhanced and delayed-phase CT, were also seen in eight patients.

Technique of Dual-Phase CBCT

An angiographic unit with a 38 × 30 cm^2 FPD (Allula Xper FD20; Philips) was used to obtain dual-phase CBCT images. Three hundred twelve projection images with X-ray parameters of 120 kV and 50–325 mA were obtained by 10.4-s acquisition with 207° rotation of the FPD of the angiographic C-arm around the patient. The radiation dose of a single CBCT measured on a CT phantom was 22.3 mGy. The first-phase was scanned during a clockwise rotation, and the second-phase was scanned during a counterclockwise rotation. The minimum interval between the end of the first scan and the start of the second scan was 4 s.

Angiography Protocol

CT during arterial portography (CBCTAP) was routinely performed at the beginning of the procedure. Forty milliliters of contrast material (370 mg I/ml iopamidol [Iopamiron 370; Bayer, Osaka, Japan] or 350 mg I/ml iomeprol [Iomeron 350; Ezai, Tokyo, Japan]) was injected at a rate of 3 ml/s through a 4F catheter placed into the superior mesenteric artery after administration of 2.5 μg prostaglandin E1 (Liple; Mitsubishi Pharma Corporation, Osaka, Japan). When replaced hepatic branches or arterial flow toward the liver from the superior mesenteric artery was demonstrated, the catheter tip was deeply advanced to avoid these branches. Scanning began 25 s after the beginning of contrast material injection, and a single-phase scan was obtained.

Dual-phase CBCTHA was obtained after CBCTAP, superior mesenteric arteriography, celiac arteriography, and common or proper hepatic arteriography. The first-phase CBCTHA was scanned during injection of 30–40 ml half-diluted contrast material at a rate of 1.5–2 ml/s through a 4F catheter placed into the common or proper hepatic artery of the liver. Scanning was initiated 7 s after the start of contrast material injection. The second-phase CBCTHA was started 30 s after the end of the first scan.

Three millimeter-thick CT-like images were obtained for observation of CBCT images on a workstation (Philips). Oxygen was administered to patients during the procedure to minimize the discomfort of breath holding.

Data Analysis

Dual-phase CBCTHA images were compared and evaluated to determine whether corona enhancement was depicted around the hypervascular tumor on the second-phase CBCTHA. Thickness of corona enhancement was also divided into two categories: thin (≤2 mm) and thick (>2 mm). The workstation did not have a measuring function; therefore, the thickness was measured using another viewer (ShadeQuest; Yokogawa Electric Corporation, Tokyo, Japan) and compared with conventional CT images. The diameters of tumors with and without corona enhancement and of tumors with thin and thick corona enhancement were statistically compared using Student t test, and $P < 0.05$ were considered significant. In addition, whether or not corona enhancement was depicted around the hypervascular pseudolesions was also evaluated.

Results

All tumors were detected as hypoattenuating lesions on CBCTAP and as hyperattenuating lesions on first-phase CBCTHA. In seven tumors showing a nodule-in-nodule appearance, the hypervascular focus on dynamic CT study was seen as hypoattenuating on CBCTAP and as hyperattenuating on first-phase CBCTHA.

Corona enhancement was detected in 63 of 71 HCC lesions (88.7%), with a mean diameter of 1.8 ± 0.9 cm (range 0.8–4.6) on second-phase CBCTHA images (Figs. 1, 2 through 3). Thin corona enhancement was seen in 18 tumors (mean diameter 1.2 ± 0.5 cm [range 0.8–2.6]), and thick corona enhancement was seen in 45 tumors (mean diameter of 2.0 ± 0.9 cm [range 0.9–4.6]). There was a significant difference in tumor diameter between thicknesses of corona enhancement ($P = 0.001$). Eight tumors with a mean diameter of 1.0 ± 0.2 cm (range 0.8–1.3) did not show any corona enhancement. There was a significant difference in tumor diameter between tumors with or without corona enhancement ($P = 0.0157$). In all seven early-stage tumors with a hypovascular portion around the hypervascular portion, corona enhancement was demonstrated around the hypervascular portion within the hypovascular tumor portion (Fig. 3).

Six (66.7%) of nine hypervascular pseudolesions showed slight diffuse enhancement on second-phase CBCTHA images. The remaining three lesions showed isoattenuation (Fig. 1). Corona enhancement was not seen in any of these lesions.

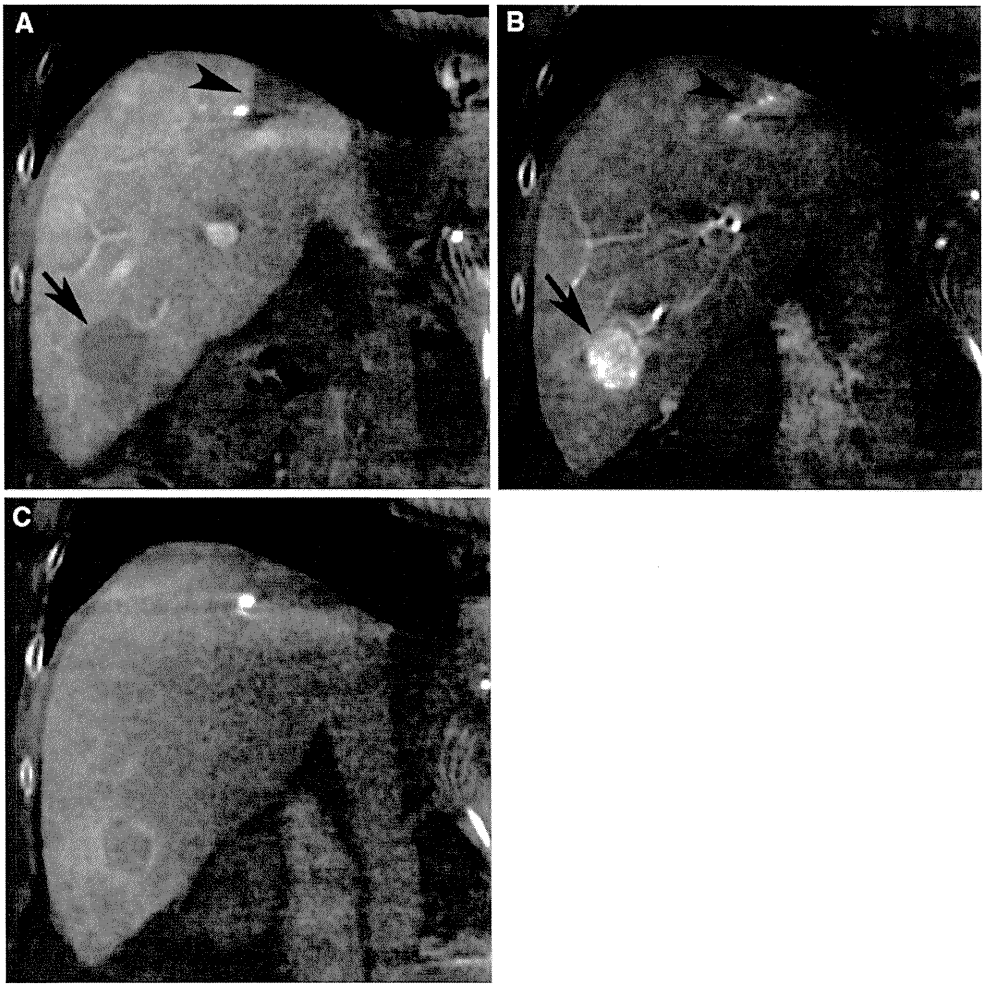

Fig. 1 HCC (2.2-cm diameter) and arterioportal shunt in the right lobe of the liver. **A** Coronal CBCTAP showed a nodular hypoattenuating lesion (HCC) (*arrow*) and wedge-shaped hypoattenuating lesion (*arrowhead*) adjacent to the tumor with iodized oil accumulation, which had previously been treated by TACE. **B** On coronal first-phase CBCTHA, HCC showed a nodular enhancement (*arrow*). The lesion near the iodized oil accumulated tumor showed wedge-shaped enhancement, including early appearance of the portal vein (*arrowhead*), suggesting an arterioportal shunt. **C** On coronal second-phase CBCTHA, thick corona enhancement was seen around the HCC nodule. The arterioportal shunt showed isoattenuation

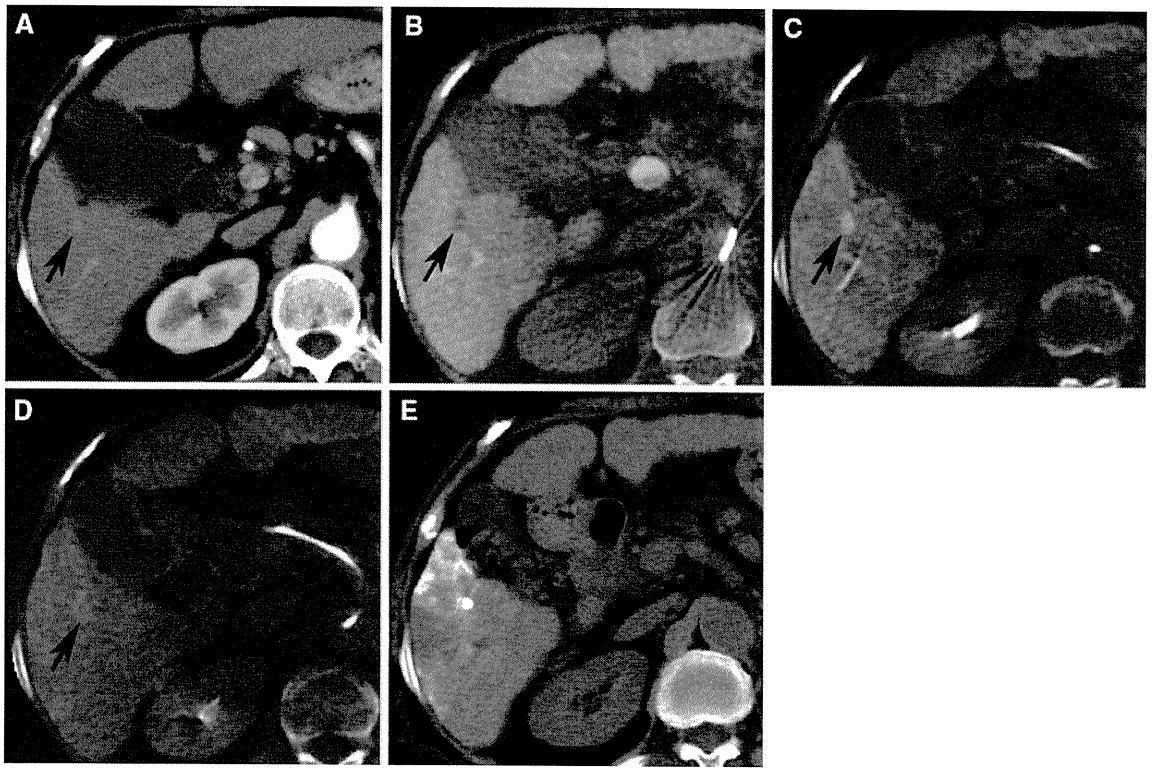

Fig. 2 Small HCC (8-mm diameter) in the right lobe of the liver. **A** Arterial-phase CT showed a small hyperattenuating lesion in the right lobe of the liver (*arrow*). **B** CBCTAP showed a nodular hypoattenuating lesion corresponding to the small lesion on CT (*arrow*). **C** On first-phase CBCTHA, the lesion showed nodular enhancement (*arrow*). **D** On second-phase CBCTHA, thin corona enhancement was seen around the lesion (*arrow*). The lesion was diagnosed as HCC and TACE was performed. **E** CT obtained 1 week after TACE showed dense iodized oil accumulation in the lesion

Discussion

Ueda et al. [1] named the wash of contrast material around hypervascular HCC lesions demonstrated on the late phase of single-level dynamic CTHA images as "corona enhancement." In a report by Kitao et al. [5], the drainage vessels of HCC change during multistep hepatocarcinogenesis. As the tumor cells become atypical and proliferate more rapidly, they first invade the intranodular hepatic veins and then compress the perinodular hepatic veins. As a result of hepatic vein occlusion, the tumor blood begins to drain into the hepatic sinusoids and portal veins. In hypervascular HCCs without a tumor capsule, direct drainage from tumor sinusoids to adjacent hepatic sinusoids is seen as thin corona enhancement ($\leq$2 mm). In hypervascular HCCs with a tumor capsule, perinodular hepatic sinusoids have collapsed, and continuity of intranodular and extranodular sinusoids is interrupted by the capsule. Therefore, tumor blood drains into the surrounding liver parenchyma through the preserved portal veins within the capsule, and thick corona enhancement (>2 mm) is demonstrated. Corona enhancement is one of the characteristic findings of hypervascular HCCs, but it is also seen around metastatic liver tumors [3, 10]. In contrast, corona enhancement is not seen around hypervasucular pseudolesions, such as arterioportal shunts. Therefore, corona enhancement is one of the most reliable findings to distinguish between liver tumors and arterioportal shunts [2].

In the present study, corona enhancement was depicted in 88.7% of HCC lesions on second-phase CBCTHA images. The minimum-diameter corona enhancement demonstrated was 0.8 cm. Thick corona enhancement was seen in relatively large tumors and might represent the rich tumor vascularity and tumor capsule formation. In addition, in seven tumors showing a nodule-in-nodule appearance, corona enhancement was seen within the hypovascular tumor portion around the hypervascular focus. This finding suggests that tumor blood of the hypervascular focus drains into the tumor sinusoids of the hypovascular portion with preserved portal vasculatures, as reported by Kita et al. [11]. This finding may also explain iodized oil accumulation in the hypovascular tumor portion after ultraselective TACE, as we previously reported [12]. Arterioportal shunts showed slightly prolonged enhancement of the entire lesion in 67% of lesions and did not show corona enhancement in any lesion. These findings helped to differentiate arterioportal shunts from hypervascular HCC lesions.

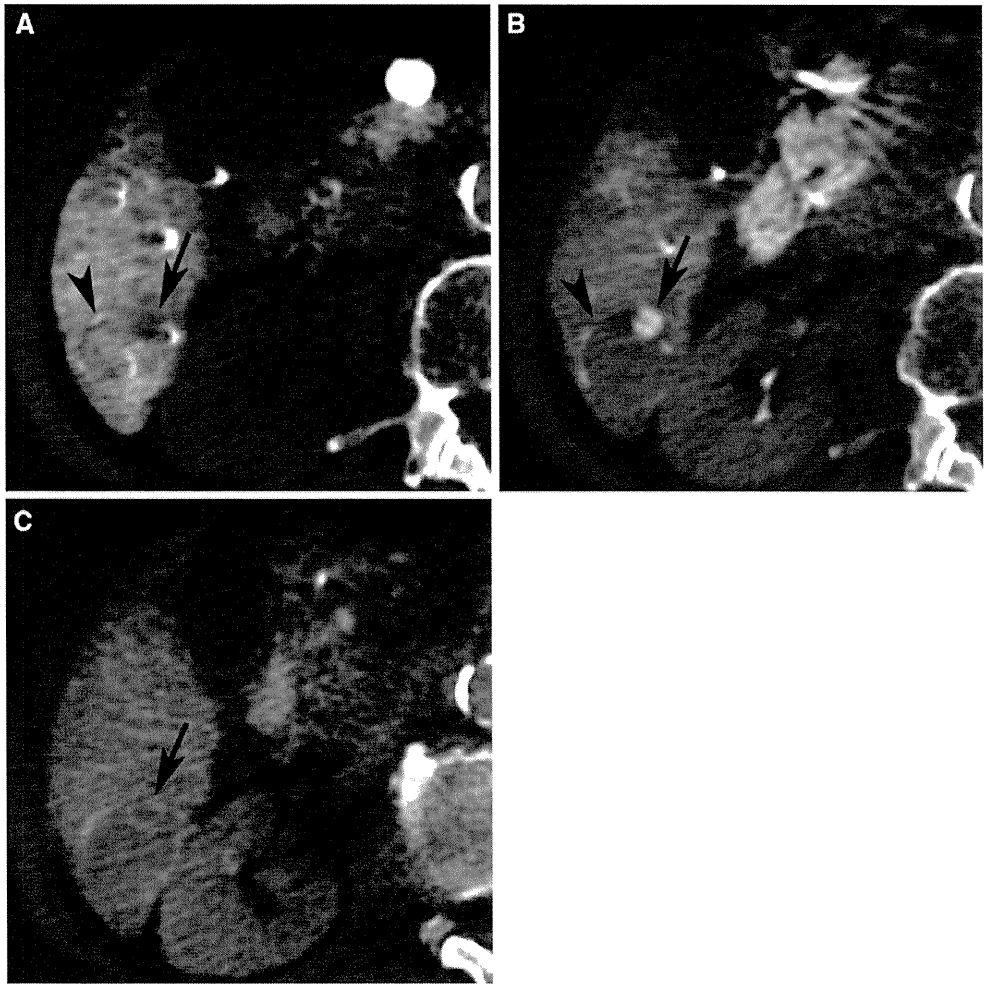

Fig. 3 Early-stage HCC, including a hypervascular focus (8-mm diameter), in the right lobe of the liver. **A** CBCTAP showed a small hypoattenuating lesion (*arrow*) in the isoattenuating nodule (*arrowhead*). **B** First-phase CBCTHA showed 3.3 cm-diameter hypoattenuating nodule (*arrowhead*), including the hypervascular focus (*arrow*). The nodule was diagnosed as early-stage HCC (nodule-in-nodule appearance). **C** Second-phase CBCTHA showed thin corona enhancement around the hypervascular focus within the hypovascular mass (*arrow*)

Inoue et al. [3] reported that corona enhancement was seen in 84% of HCC lesions and 73% of metastatic liver tumors and cholangiocarcinomas on late-phase conventional CTHA images. Our findings suggest that dual-phase CBCTHA has an ability to detect corona enhancement of HCC lesions that is almost equal to conventional CTHA; however, the spatial and contrast resolution of CBCT is inferior to that of conventional multidetector CT. We injected a larger amount of contrast material for dual-phase CBCTHA than that for single-phase CBCTHA [9] to facilitate the depiction of corona enhancement. This additional contrast material might have improved the detectability of corona enhancement on CBCTHA.

There are some limitations to the present study. First, corona enhancement was only evaluated on CBCTHA images, and conventional CTHA images were not obtained in any tumor. Therefore, absence of corona enhancement may not directly indicate that the tumor does not have obvious tumor drainage. Because all hypervascular HCC lesions may have tumor drainage around the surrounding liver parenchyma, we speculate that the absence of corona enhancement on second-phase CBCTHA images, especially in small tumors, may be influenced mainly by the degree of tumor vascularity and image quality of CBCT. Second, histological confirmation was not obtained in any of the tumors. However, we consider that advances in imaging modalities have facilitated the establishment of HCC diagnosis without biopsy. Third, we could not confirm whether tumors showing thick corona enhancement had a tumor capsule because all tumors were treated by TACE alone. Fourth, all arterioportal shunts in the present study were large and presented typical imaging findings; therefore, we could not conclude that small arterioportal shunts could be adequately differentiated from small HCC

lesions by dual-phase CBCTHA technique. However, we consider dual-phase CBCTHA technique useful to distinguish small HCCs from hypervascular pseudolesions.

In conclusion, dual-phase CBCTHA can depict corona enhancement around almost all hypervascular HCC lesions. This technique may improve the diagnostic accuracy of HCC by CBCTHA.

References

1. Ueda K, Matsui O, Kawamori Y et al (1998) Hypervascular hepatocellular carcinoma: evaluation of hemodynamics with dynamic CT during hepatic arteriography. Radiology 206:161–166
2. Ueda K, Matsui O, Kawamori Y et al (1998) Differentiation of hypervascular hepatic pseudolesions from hepatocellular carcinoma: value of single-level dynamic CT during hepatic arteriography. J Comput Assist Tomogr 22:703–708
3. Inoue E, Fujita M, Hosomi N et al (1998) Double phase CT arteriography of the whole liver in the evaluation of hepatic tumors. J Comput Assist Tomogr 22:64–68
4. Matsui O, Ueda K, Kobayashi S et al (2002) Intra- and perinodular hemodynamics of hepatocellular carcinoma: CT observation during intra-arterial contrast injection. Abdom Imaging 27:147–156
5. Kitao A, Zen Y, Matsui O et al (2009) Hepatocarcinogenesis: multistep changes of drainage vessels at CT during arterial portography and hepatic arteriography—radiologic-pathologic correlation. Radiology 252:605–614
6. Hirota S, Nakao N, Yamamoto S et al (2006) Cone-beam CT with flat-panel-detector digital angiography system: early experience in abdominal interventional procedures. Cardiovasc Intervent Radiol 29:1034–1038
7. Kakeda S, Korogi Y, Ohnari N et al (2008) Usefulness of cone-beam CT with flat panel detectors in conjunction with catheter angiography for transcatheter arterial embolization. J Vasc Interv Radiol 18:1508–1516
8. Miyayama S, Matsui O, Yamashiro M et al (2009) Detection of hepatocellular carcinoma by CT during arterial portography using a cone-beam CT technology: comparison with conventional CTAP. Abdom Imaging 34:502–506
9. Miyayama S, Yamashiro M, Okuda M et al (2009) Usefulness of cone-beam computed tomography during ultraselective transcatheter arterial chemoembolization for small hepatocellular carcinomas that cannot be demonstrated on angiography. Cardiovasc Intervent Radiol 32:255–264
10. Terayama N, Matsui O, Ueda K et al (2002) Peritumoral rim enhancement of liver metastasis: hemodynamics observed on single-level dynamic CT during hepatic arteriography and histopathologic correlation. J Comput Assist Tomogr 26:975–980
11. Kita R, Nishikawa H, Matsuo H et al (2007) A case of nodule-in-nodule type HCC presenting corona enhancement within the outer tumor on single-level dynamic CT during hepatic arteriography. Nihon Shokakibyo Gakkaishi 104:837–839 (in Japanese)
12. Miyayama S, Matsui O, Yamashiro M et al (2007) Iodized oil accumulation in the hypovascular tumor portion of early-stage hepatocellular carcinoma after ultraselective transcatheter arterial chemoembolization. Hepatol Int 1:451–459

Cardiovasc Intervent Radiol (2011) 34:1244–1253
DOI 10.1007/s00270-010-0036-3

CLINICAL INVESTIGATION

Angiographic Evaluation of Feeding Arteries of Hepatocellular Carcinoma in the Caudate Lobe of the Liver

Shiro Miyayama · Masashi Yamashiro · Yuki Hattori · Nobuaki Orito · Ken Matsui · Kazunobu Tsuji · Miki Yoshida · Osamu Matsui

Received: 12 July 2010 / Accepted: 24 October 2010 / Published online: 18 November 2010

Abstract
Purpose To evaluate the origins of feeders of hepatocellular carcinoma (HCC) in the caudate lobe (S1).
Materials and Methods Eighty-eight HCCs (mean diameter 21.4 mm) were treated by chemoembolization. The tumor-feeding caudate artery was confirmed when a tumor stain was demonstrated on angiogram and iodized oil was accumulated into the HCC and S1 on computed tomography (CT). The origins were divided into R_1 (right proximal), R_2 (right distal), L_1 (left proximal), L_2 (left distal), A (anterior segmental), P (posterior segmental), M (middle hepatic or medial segmental), Ph (proper hepatic), Ch (common hepatic), and Ex (extrahepatic). The origins of feeders supplying HCCs in the Spiegel lobe (SP; $n = 36$), the paracaval portion (PC; $n = 38$), and the caudate process (CP; $n = 14$) were also analyzed.
Results One hundred sixteen feeders were identified: 11 (9.5%) arose from R_1; 21 (18.1%) arose from R_2; nine arose (0.9%) from L_1; 15 (12.9%) arose from L_2; 24 (20.7%) arose from A; 25 (21.6%) arose from P; seven (6.0%) arose from M; one (0.9%) arose from Ph; and three (2.6%) arose from Ex. HCCs in the SP and the PC were fed by feeders from both hepatic arteries (the ratios of right to left were 3:2 and 3:1, respectively), and HCCs in the CP were dominantly fed by feeders from the right hepatic artery.
Conclusion The caudate artery most frequently arises from the right hepatic artery, followed with almost equal frequency by the left hepatic, the anterior segmental, and the posterior segmental artery. The origins of the caudate arteries differ according to the subsegmental locations.

Keywords Hepatocellular carcinoma · Caudate lobe · Feeding artery · Transcatheter arterial chemoembolization

S. Miyayama (✉) · M. Yamashiro · Y. Hattori · N. Orito · K. Matsui · K. Tsuji · M. Yoshida
Department of Diagnostic Radiology, Fukuiken Saiseikai Hospital, Fukui, Japan
e-mail: s-miyayama@fukui.saiseikai.or.jp

O. Matsui
Department of Radiology, Kanazawa University Graduate School of Medical Science, Kanazawa, Japan

Introduction

The caudate lobe is centrally located in the liver between the right and left lobes of the liver and near the hepatic hilus and the inferior vena cava. Because of this anatomic location, hepatocellular carcinoma (HCC) arising in the caudate lobe is difficult to treat [1]. Surgical resection of the caudate lobe has a high mortality rate because of large amounts blood loss, a high rate of postoperative complications, and a high tumor-recurrence rate [2, 3]. Percutaneous ablation therapy, such as ethanol injection and radiofrequency ablation, is a useful alternative treatment [4–6]; however, the procedure might be technically difficult because of the deep tumor location and adjacent large vessels. Therefore, transcatheter arterial chemoembolization (TACE) plays an important role in the treatment of HCC in the caudate lobe, although local tumor recurrence is frequently observed after TACE [4, 7, 8].

Because there are usually multiple caudate arteries arising from the right, left, and middle hepatic arteries, as well as from the extrahepatic collateral vessels, 16–31% of HCCs in the caudate lobe are fed by multiple branches arising from different origins [7–12]. These factors might make it more difficult to control HCC in the caudate lobe using TACE [7, 8, 10]. Recognition of vascular anatomy

supplying HCCs in the caudate lobe is key to performing effective TACE. Thus, the purpose of our study was to retrospectively analyze the origins of the HCC-feeding arteries in the caudate lobe and to evaluate the anatomic variations of tumor-feeding arteries in relation to subsegments of the caudate lobe.

Materials and Methods

We performed a retrospective study to evaluate the origins of tumor-feeding caudate arteries. This was a retrospective study using imaging data and clinical records with no change in patient care; Institutional Review Board approval is not required at our institution for this type of study. Written informed consent was obtained from each patient before the TACE procedure.

Patients

Between February 2002 and February 2010, 88 HCCs originating in the caudate lobe were detected in 84 patients. There were 48 men and 36 women, and the mean patient age was (mean ± SD) 70.2 ± 7.3 years (range 45–86). All patients had liver cirrhosis. This was related to hepatitis C in 71 patients, to hepatitis B in four patients, and to alcohol in three patients. The etiology was unknown in six patients. The diagnosis of HCC was established by imaging findings: (1) characteristic nodular enhancement on the arterial phase and wash out on the delayed phase images on computed tomography (CT) and/or magnetic resonance imaging; (2) nodular stain on angiography and/or CT during hepatic arteriography obtained using conventional CT or cone-beam CT; and (3) nodular perfusion defect on CT during arterial portography obtained using conventional CT or cone-beam CT. Histological confirmation was not obtained in any patient in this series. Mean tumor diameter was 21.4 ± 11.0 mm (range 8–62). Fifty-two patients (61.9%) had a history of TACE for HCC before detection of HCC in the caudate lobe. Thirty-two patients (38.1%) had no treatment history for HCC.

Hepatic Angiography and the TACE Procedure

Arteriograms of the celiac and superior mesenteric arteries were routinely performed using a 4F catheter. Common hepatic or proper hepatic arteriogram was also performed in all patients using a 4F catheter or a 1.8F-tip (Carnelian Pixie; Tokai Medical Products, Kasugai, Japan), a 2F-tip (Progreat α; Terumo, Tokyo, Japan), or a 2.4F-tip (Microferret; Cook, Bloomington, IN, USA) microcatheter. Arteriograms of extrahepatic vessels, such as the right inferior phrenic artery, the right renal capsular artery, and the left gastric artery, were obtained when the tumor stain was unclear on hepatic arteriography.

All TACE procedures performed through the caudate arteries were selectively performed using a microcatheter. The microcatheter with its tip bent into a J shape by steam was used for all procedures to facilitate insertion into small caudate arteries that branched at acute angles. To navigate the microcatheter, a 0.016-inch guidewire (GT-wire; Terumo) was used. When selection of the feeding branch by the 0.016-inch guidewire was difficult, a 0.012-inch guidewire (GT-wire; Terumo) was used. After the microcatheter was inserted into the target branch, 0.5 ml 2% lidocaine (Xylocaine; Fujisawa, Osaka, Japan) was intra-arterially injected to prevent pain and vasospasm. First, a mixture of 2–4 ml iodized oil (Lipiodol; Andre Guerbet, Aulnaysous-Bois, France) and anticancer drugs (10–20 mg epirubicin [Farmorbicin; Kyowa Hakko, Tokyo, Japan] and 2–4 mg mitomycin C [Mitomycin; Kyowa Hakko]) was injected and this was followed by injection of gelatin sponge particles. The total amount of iodized oil injected in a single procedure was determined based on the tumor size (volume almost equal to the diameter of the tumor, e.g., a 3-cm tumor received 3 ml iodized oil). Until December 2006, gelatin sponge (Gelfoam; Upjohn, Kalamazoo, MI, USA) particles that were cut into approximately 1-mm cubes were used. Since January 2007, commercially available gelatin sponge particles (Gelpart; Nippon Kayaku, Tokyo, Japan) 1 mm in diameter have been used. TACE through extrahepatic collateral vessels was also performed when the blood supply to the tumor was demonstrated. Unenhanced CT was obtained 1 week after TACE in all patients to check for iodized oil accumulation in HCCs in the caudate lobe.

Definition of the Origin of the Caudate Artery

We defined the embolized branch as the tumor-feeding caudate artery when a tumor stain was demonstrated on arteriogram and iodized oil showed accumulation in the HCC and the caudate lobe on CT obtained 1 week after TACE. If CT 1 week after TACE showed a tumor portion in which iodized oil was not accumulated, an additional TACE was performed 2–6 months later according to the residual tumor size and patient's medical condition. When the residual tumor was supplied by another caudate artery that had initially not been embolized, the caudate artery was also defined as the tumor-feeding caudate artery.

The origins of the caudate arteries were divided into R_1, R_2, L_1, L_2, A, P, M, Ph, Ch, and Ex (Fig. 1). The caudate lobe was divided into three subsegments according to the classification proposed by Kumon [13] (Fig. 2): the Spiegel lobe (SP), the paracaval portion (PC), and the caudate process (CP). The origins of the caudate arteries supplying

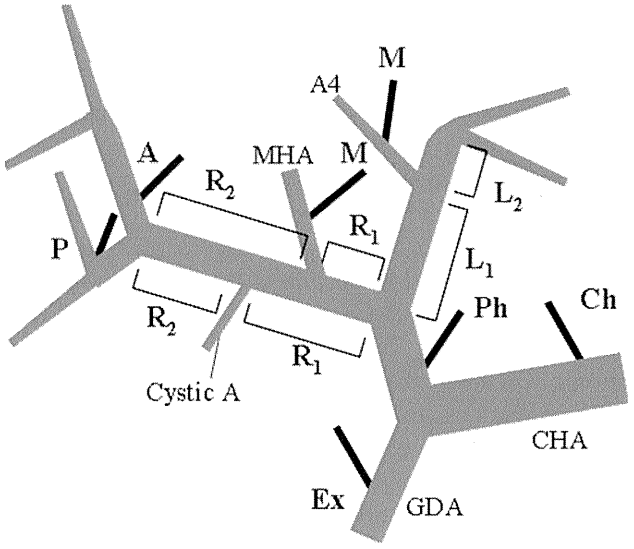

Fig. 1 The definition of the origins of tumor-feeding caudate arteries. R_1 (*right proximal*) arising from the right hepatic artery (RHA) between its origin and the middle hepatic artery (MHA) bifurcation or the cystic artery bifurcation if the MHA was not present; R_2 (*right distal*) arising from the RHA between the MHA (or cystic artery) bifurcation and the bifurcation of the anterior and posterior segmental artery of the RHA. If both the MHA and the cystic artery were not present, the RHA was divided into the two equal parts; L_1 (*left proximal*) arising from the left hepatic artery (LHA) between its origin and the medial segmental artery (A4) bifurcation; L_2 (*left distal*) arising from the LHA between the A4 bifurcation and the umbilical portion of the LHA. If the A4 did not arise from the LHA, the LHA was divided into the two equal parts; *A* arising from the anterior segmental artery of the right hepatic artery; *P* arising from the posterior segmental artery of the right hepatic artery; *M* arising from the MHA or the A4; *Ph* arising from the proper hepatic artery; *Ch* arising from the common hepatic artery; and *Ex* arising from the extrahepatic vessels

the HCCs in each subsegment were also analyzed. When a tumor was located between two subsegments, the tumor was classified based on the one subsegment in which it was dominantly located.

Results

Origins of the Tumor-Feeding Caudate Arteries

Eighty-two tumors in the caudate lobe of 78 patients were treated by a single TACE session. The remaining six tumors in six patients were treated with two TACE sessions because of incomplete iodized oil accumulation in the entire tumor on CT obtained after the initial TACE session. In total, 116 caudate arteries were identified, and all were selectively embolized during TACE, including six additional TACE sessions (Table 1). During TACE, 1.3 ± 0.5 feeding arteries (range 1–3) were embolized/tumor. Eleven caudate arteries (9.5%) were derived from R_1; 21 (18.1%) from R_2; nine (7.8%) from L_1; 15 (12.9%) from L_2; 24 (20.7%) from A; 25 (21.6%) from P; seven (6.0%) from M; one (0.9%) from Ph; and three (2.6%) from Ex. No caudate arteries were derived from Ch in the present series. Eighty-one caudate arteries (70.4%) were derived from the right hepatic arterial system ($R_1 + R_2 + A + P$), and 31 (27.0%) were derived from the left hepatic arterial system ($L_1 + L_2 + M$). In total, 27.6% of the caudate arteries were derived from the right hepatic artery ($R_1 + R_2$), 20.7% from the left hepatic artery ($L_1 + L_2$), 20.7% from the anterior segmental artery of the right hepatic artery, 21.6% from the posterior segmental artery of the right hepatic artery, and 6.0% from the middle hepatic artery or the medial segmental artery.

Origins of the Caudate Arteries Supplying HCCs in the SP

Our findings are listed in Table 2. There were 36 tumors with a mean diameter of 22.3 ± 11.9 mm (range 8–62 mm) in the SP. Twenty-five tumors (69.4%) were supplied by a single tumor-feeding caudate artery. Among these, 15 tumors were supplied by the feeding artery derived from the right hepatic arterial system (R_1 [$n = 2$], R_2 [$n = 7$], A [$n = 2$], P [$n = 4$]) (Fig. 3), and nine were supplied by the feeding artery derived from the left hepatic arterial system (L_1 [$n = 3$], L_2 [$n = 4$], M [$n = 2$]). The remaining tumor was supplied by a feeding artery derived from the right inferior phrenic artery (Ex). Eleven tumors (30.6%) had two feeding arteries. Among these, eight were supplied by feeding arteries derived from the right (R_1 [$n = 2$], R_2 [$n = 1$], A [$n = 4$], P [$n = 1$]) and the left hepatic arterial system (L_1 [$n = 3$], L_2 [$n = 4$], M [$n = 1$]), respectively (Figs. 4 and 5). One tumor was supplied by two feeding arteries derived from A. The remaining two tumors were supplied by feeding arteries derived from the left hepatic arterial system (L_2 [$n = 1$], M [$n = 1$]) and Ex (the right inferior phrenic artery [$n = 1$] as well as the accessory left gastric artery [$n = 1$]), respectively. In total, there were 47 tumor-feeding caudate arteries. Twenty-five tumor-feeding arteries arose from the right hepatic arterial system, 19 from the left hepatic arterial system, and three from the extrahepatic collaterals. The diameters of three tumors that were supplied by extrahepatic collaterals were 17, 26, and 48 mm, respectively. All three tumors were detected in patients with no histories of TACE, including one patient who had undergone hepatic resection. All three tumors were located at the anterior ($n = 1$) or posterior ($n = 2$) surface of the SP.